DOI: 10.1002/chem.200600269

# Mechanistic Investigation of the Oxygen-Atom-Transfer Reactivity of Dioxo-molybdenum(VI) Complexes

**Brian W. Kail,[a] Lisa M. Pérez,[b] Snežana D. Zarić,[c] Andrew J. Millar,[d] Charles G. Young,*[d] Michael B. Hall,*[b] and Partha Basu*[a]**

**Abstract:** The oxygen-atom-transfer (OAT) reactivity of [$L^{iPr}MoO_2(OPh)$] (**1**, $L^{iPr}$ = hydrotris(3-isopropylpyrazol-1-yl)borate) with the tertiary phosphines $PEt_3$ and $PPh_2Me$ in acetonitrile was investigated. The first step, [$L^{iPr}MoO_2(OPh)$]+$PR_3$ → [$L^{iPr}MoO(OPh)(OPR_3)$], follows a second-order rate law with an associative transition state ($PEt_3$, $\Delta H^{\neq}=48.4$ ($\pm1.9$) kJ mol$^{-1}$, $\Delta S^{\neq}=-149.2$ ($\pm6.4$) J mol$^{-1}$ K$^{-1}$, $\Delta G^{\neq}=92.9$ kJ mol$^{-1}$; $PPh_2Me$, $\Delta H^{\neq}=73.4$ ($\pm3.7$) kJ mol$^{-1}$, $\Delta S^{\neq}=-71.9$ ($\pm2.3$) J mol$^{-1}$ K$^{-1}$, $\Delta G^{\neq}=94.8$ kJ mol$^{-1}$). With $PMe_3$ as a model substrate, the geometry and the free energy of the transition state (TS) for the formation of the phosphine oxide-coordinated intermediate were calculated. The latter, 95 kJ mol$^{-1}$, is in good agreement with the experimental values. An unexpectedly large O-P-C angle calculated for the TS suggests that there is significant O-nucleophilic attack on the P–C σ* in addition to the expected nucleophilic attack of the P on the Mo=O π*. The second step of the reaction, that is, the exchange of the coordinated phosphine oxide with acetonitrile, [$L^{iPr}MoO(OPh)(OPR_3)$] + MeCN → [$L^{iPr}MoO(OPh)(MeCN)$] + $OPR_3$, follows a first-order rate law in MeCN. A dissociative interchange ($I_d$) mechanism, with activation parameters of $\Delta H^{\neq}=93.5$ ($\pm0.9$) kJ mol$^{-1}$, $\Delta S^{\neq}=18.2$ ($\pm3.3$) J mol$^{-1}$ K$^{-1}$, $\Delta G^{\neq}=88.1$ kJ mol$^{-1}$ and $\Delta H^{\neq}=97.9$ ($\pm3.4$) kJ mol$^{-1}$, $\Delta S^{\neq}=47.3$ ($\pm11.8$) J mol$^{-1}$ K$^{-1}$, $\Delta G^{\neq}=83.8$ kJ mol$^{-1}$, for [$L^{iPr}MoO(OPh)(OPEt_3)$] (**2a**) and [$L^{iPr}MoO(OPh)(OPPh_2Me)$] (**2b**), respectively, is consistent with the experimental data. Although gas-phase calculations indicate that the Mo–$OPMe_3$ bond is stronger than the Mo–NCMe bond, solvation provides the driving force for the release of the phosphine oxide and formation of [$L^{iPr}MoO(OPh)(MeCN)$] (**3**).

**Keywords:** atom-transfer reactions · bioinorganic chemistry · kinetics · molybdoenzymes · reaction mechanisms

## Introduction

The transfer of oxygen, nitrogen, or sulfur atoms between competent centers is a fundamental reaction in chemistry and biology, and during the past decades these reactions have been extensively studied.[1–5] The majority of the oxygen-atom-transfer (OAT) reactions involve high-valent metal centers, and the transfer of an oxygen atom to the acceptor is coupled to the transfer of an electron pair to the donor [Eq. (1)]. Although the exact nature of the reaction may vary, OAT reactions are thought to be involved in the mechanisms of several metalloenzymes, such as cytochrome P450, sulfite oxidase, nitrate reductase, and dimethyl sulfoxide (DMSO) reductase. Catalytic transfer of oxygen atoms is also important in industrial processes, such as the epoxidation of olefins.[6,7]

$$[MO]^{n+}+X \rightleftharpoons [M]^{(n-2)+}+XO \quad (1)$$

Due to their biological and industrial relevance, OAT reactions involving high-valent oxo-molybdenum complexes

[a] B. W. Kail, Prof. P. Basu
Department of Chemistry and Biochemistry, Duquesne University
Mellon Hall, Pittsburgh, PA 15282 (USA)
Fax: (+1) 412-396-5683
E-mail: basu@duq.edu

[b] Dr. L. M. Pérez, Prof. M. B. Hall
Department of Chemistry, Texas A&M University College Station
Texas 77843–3255 (USA)
E-mail: mbhall@tamu.edu

[c] Prof. S. D. Zarić
Department of Chemistry, University of Belgrade
Studentski trg 16, P.O. Box 158, 11001 Belgrade (Serbia)

[d] Dr. A. J. Millar, Prof. C. G. Young
School of Chemistry, University of Melbourne
Victoria 3010 (Australia)
E-mail: cgyoung@unimelb.edu.au

Supporting information for this article is available on the WWW under http://www.chemeurj.org/ or from the author: Figure S1 shows the original and reconstructed optical spectra with residual, Figure S2 Arrhenius and Eyring plots for the intermediate formation and solvent coordination. Rate constants are tabulated in Tables S1 and S2.

  

have been extensively investigated.[8–11] Oxo-molybdenum complexes containing dithiocarbamate,[12] ene dithiolate,[13–15] and hydrotris(pyrazolyl)borate[16,17] ligands feature in the more notable, functional OAT systems. Both $Mo^{VI}O_2/Mo^{IV}O$ and $Mo^{VI}O/Mo^{IV}$ couples have been reported to effect substrate oxidation and reduction. For many years, a variety of biological substrates were used in model systems, however, tertiary phosphines have become the reagents of choice, due to their high solubility in organic solvents and the ability to tune their reactivity through substitution at phosphorus.

A long-standing mechanistic description of OAT from dioxo-$Mo^{VI}$ centers to tertiary phosphines involves nucleophilic attack by the phosphine on an empty Mo=O $\pi^*$ orbital. In these reactions, the existence of a single transition state was supported by experimental data. However, a computational investigation indicated that one such reaction proceeds via the formation of a phosphine oxide-coordinated intermediate.[18] The other oxo group acts in a "spectator" capacity, as described by Rappé and Goddard.[19] Experimental evidence for the proposed intermediate was provided through the in situ detection of species of the general formula [LMoO($OPPh_3$)X], in which L = hydrotris(3,5-dimethylpyrazol-1-yl)borate; $X^- = SPh^-$, $OPh^-$, $Br^-$, and $Cl^-$.[20] Confirmation of the existence of OAT intermediates came through the isolation and structural characterization of [$L^{iPr}$MoO($OPR_3$)X] ($L^{iPr}$ = hydrotris(3-isopropylpyrazol-1-yl)borate; X = $Cl^-$, substituted phenolate, or alkyl thiolate)[20–22] and [LMoO($OPMe_3$)Cl].[23,24] This L system models for the reduction of DMSO by DMSO reductase and the oxidation of sulfite by sulfite oxidase, in which a catalytically labile oxygen atom is passed from the enzyme to the substrate with the concomitant transfer of two electrons.[25] Recent calculations have predicted similar intermediates in other oxo-transfer model systems.[26,27]

Here, we describe a detailed kinetics investigation of the formation and subsequent solvation of [$L^{iPr}$MoO(OPh)($OPR_3$)] (**2**; $R_3 = Et_3$ (**2a**) and $Ph_2Me$ (**2b**)) en route from [$L^{iPr}MoO_2$(OPh)] (1)/$PR_3$ to [$L^{iPr}$MoO(OPh)-(NCMe)] (**3**)/$OPR_3$ in acetonitrile, and provide an experimental analysis of the rate-limiting nature in these two steps. The experimental results are supported by theoretical calculations of the geometries and energies of the intermediates involved in these reactions and the transition states connecting them.

## Results

**Kinetics of the reaction of [$L^{iPr}MoO_2$(OPh)] (1) with $PR_3$**: Solutions of yellow-orange **1** react with $PEt_3$ and $PPh_2Me$ to produce green solutions containing the isolable oxo(phosphoryl)-$Mo^{IV}$ complexes, **2**.[20,21] These reactions follow a second-order rate law, dependent on both the complex and the phosphine (Figure 1, step 1). The products exhibit two low-energy d–d transitions that are absent from the starting materials. The lowest-energy transition is observed at around 910 nm ($\varepsilon \sim 110\,M^{-1}cm^{-1}$) for **2a**, and at 900 nm ($\varepsilon \sim 92\,M^{-1}cm^{-1}$) for **2b**. Reactions with (phosphine:Mo complex) mole ratios higher than ~60 and 90 for $PEt_3$ and $PPh_2Me$, respectively, appear to be too rapid to be quantifiable, and as such, were used as an upper limit of the concentration ratio. The pseudo-first-order rate constants as a function of the concentration of phosphines and at different temperatures are given in the Supporting Information; the activation parameters are tabulated in Table 1. The large negative entropies of activation, $(T\Delta S^{\ddagger})_{PEt_3} = -44.5\,kJ\,mol^{-1}$ and $(T\Delta S^{\ddagger})_{PPh_2Me} = -21.4\,kJ\,mol^{-1}$ at 298.15 K, are consistent with associative transition states for both phosphine reactions.

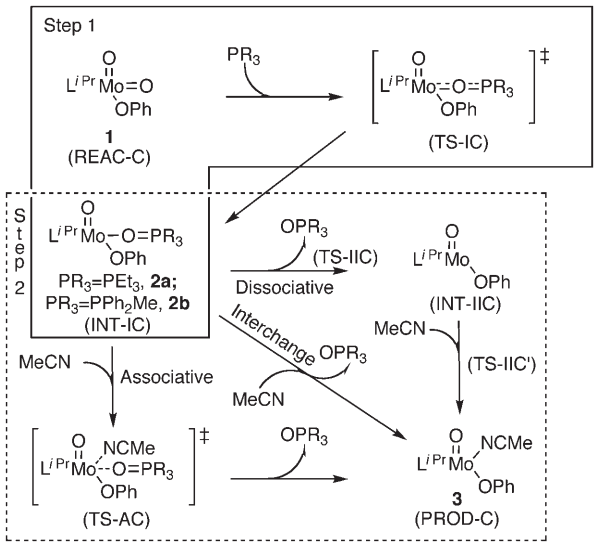


Figure 1. Schematic representation of the oxygen-atom-transfer reaction path. The two kinetically defined steps are shown in separate boxes. Compounds **1**, **2**, and **3** were experimentally characterized. Labels ending in C refer specifically to the theoretically calculated species for which R = $CH_3$.

**Kinetics of loss of $OPR_3$ from 2 in acetonitrile**: The singular value decomposition (SVD) analyses indicate that the solvation of **2a** by MeCN at 11 °C involves three observable spe-

Table 1. Activation parameters.[a]

| Reaction | $\Delta H^{\ddagger}$ [kJ mol$^{-1}$] | $\Delta S^{\ddagger}$ [J mol$^{-1}$ K$^{-1}$] | ln$A$ | $E_a$ [kJ mol$^{-1}$] | $\Delta G^{\ddagger}$ [kJ mol$^{-1}$], 298 K |
|---|---|---|---|---|---|
| **1**+$PEt_3$→**2a** | 48.4 (1.9) | −149.2 (6.4) | 12.5 (0.8) | 50.9 (1.9) | 92.9 |
| **1**+$PPh_2Me$→**2b** | 73.4 (3.7) | −71.9 (2.3) | 21.8 (1.5) | 75.9 (3.8) | 94.8 |
| **2a**+MeCN→**3**+$OPEt_3$ | 93.5 (0.9) | 18.2 (3.3) | 31.3 (0.4) | 95.9 (0.9) | 88.1 |
| **2b**+MeCN→**3**+$OPPh_2Me$ | 97.9 (3.4) | 47.3 (11.8) | 36.1 (1.4) | 100.3 (3.4) | 83.8 |

[a] The errors in parentheses are estimated standard deviations from linear least-squares fit.

  

cies, with an initial, comparatively rapid increase of a species followed by a slower decay to another species. The first step involves solvation by acetonitrile, the second step is postulated to be the formation of a dinuclear compound. The formation of dinuclear species are well known in the literature and we focus here on the solvated species formation. The solvation reaction was probed by recording single-wavelength measurements. The absorbance changes at 301 nm and 910 nm were assigned to the decay of **2a** to **3** and fit well to a single exponential. The d–d transitions at 910 nm mirror the changes that occur in the pπ to dπ charge-transfer transitions at 301 nm. On the other hand, the absorbance changes at 680 nm were fitted to a two-exponential function. The first of the two processes corresponds to the conversion of **2a** to **3** and the second one was assigned to the formation of a dinuclear species. Because the concentrations used in the single-wavelength measurements at 301, 680, and 910 nm differ by nearly an order of magnitude, the rate of the reaction does not appear to be concentration dependent. Figure 2 shows representative data with fits at each of the wavelengths. The activation parameters (Table 1) were determined from the reaction-rate data at variable temperature. For **2a** and **2b**, the second step of Figure 1 is a dissociative process (see below), determined by the positive entropy of activation: at 298 K, $T\Delta S^{\neq}$ is 5.4 and 14.1 kJ mol$^{-1}$ for **2a** and **2b**, respectively.

**Identification of the species formed**: The solvation of **2a** was further probed by performing $^{1}$H and $^{31}$P NMR spectroscopy in benzene and in MeCN. The $^{31}$P NMR spectra in [D$_6$]benzene show conversion of coordinated phosphine oxide ($\delta = 74$ ppm) to the free form ($\delta = 48$ ppm). $^{31}$P NMR spectra of **2a**, acquired at −40 °C in [D$_3$]MeCN, showed that over time, the signal of the coordinated OPEt$_3$[20] was replaced with that of uncoordinated OPEt$_3$. The rate of phosphine oxide dissociation was calculated from the integrated intensity of both the free and the coordinated OPEt$_3$ resonances. NMR spectra of solutions incubated at 11 °C showed an increase in free OPEt$_3$ that follows a single exponential process with a half-life of ~50 min in MeCN, which is in good agreement with the single-wavelength spectrophotometric measurements. Thus, $^{31}$P NMR spectra provide direct evidence for the loss of phosphine oxide during the first step in the solvation of **2a** to **3**. Interestingly, $^{1}$H NMR spectra of compound **3** recorded at room temperature in [D$_3$]MeCN containing 10% MeCN exhibit a broad resonance at $\delta$ 2.99 ppm. We attribute the broadness to the exchange with the bulk solvent, as observed in a similar system.[24] Green **2a**, which exhibits an absorption at 910 nm ($\varepsilon = 120\,\text{M}^{-1}\text{cm}^{-1}$) from a $d_{xy} \rightarrow d_{xz}/d_{yz}$ transition, rapidly converts to blue **3**, exhibiting two $d_{xy} \rightarrow d_{xz}/d_{yz}$ transitions at 680 nm ($\varepsilon = \sim 90\,\text{M}^{-1}\text{cm}^{-1}$) and 910 nm ($\varepsilon = \sim 100\,\text{M}^{-1}\text{cm}^{-1}$).[22,24]

**Effect of solvent**: The formation and solvation of complex **2a** was investigated in different solvents. The formation reaction, probed in MeCN and benzene, showed a solvent dependence, the second-order rate constants at 17 °C being

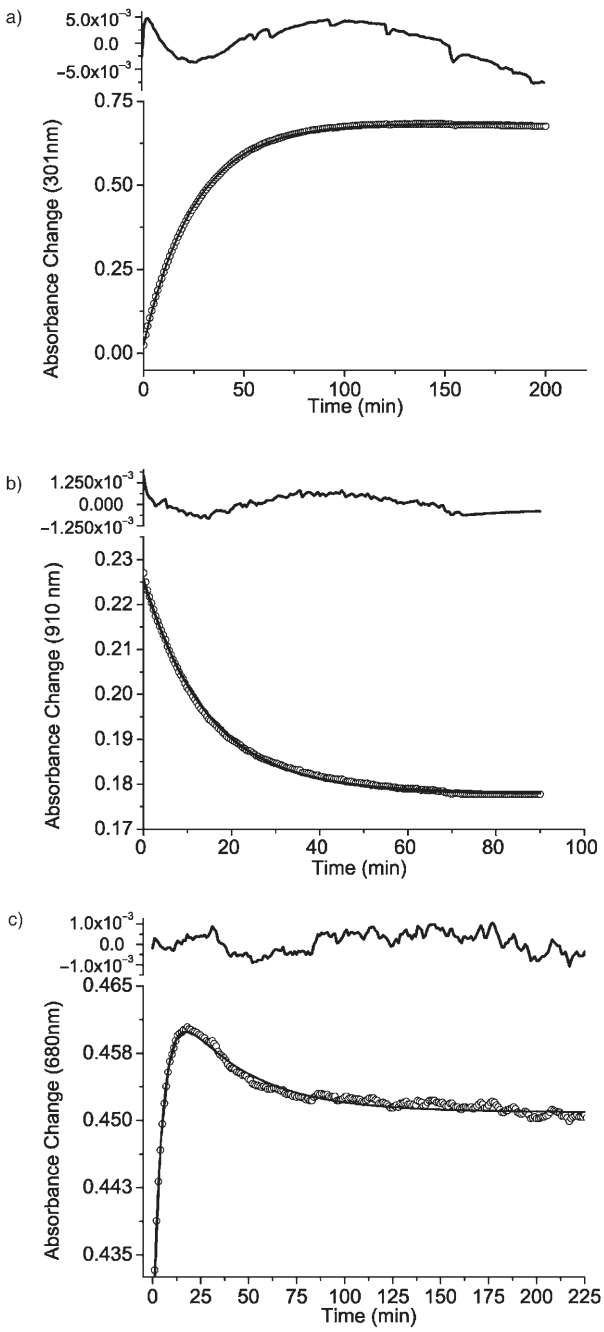


Figure 2. Observed changes in the absorption for the solvation of [L$^{i\text{Pr}}$MoO(OPh)(OPEt$_3$)] in MeCN: a) 301 nm at 16 °C, b) 910 nm at 22 °C, and c) 680 nm at 27 °C. Bottom traces represent the kinetic fit, top traces represent the residual.

$4.72 \times 10^{-2}$ and $2.75 \times 10^{-2}\,\text{M}^{-1}\text{sec}^{-1}$, respectively. Thus, the rate of the intermediate formation (Figure 1, INT-IC) in MeCN is approximately two-fold faster than it is in benzene.

The loss of OPEt$_3$ from **2a** was investigated in MeCN, benzene, and THF. In THF, the d–d transitions shift ~25 cm$^{-1}$ higher in energy relative to those observed in MeCN, which allows the observation of both solvolysis and dinucleation reactions in this region. For step 2 of Figure 1, a comparison of the apparent rates in MeCN and THF

  

shows that they are equivalent within statistical error (rate constant $\sim 6.3 \times 10^{-2}\ min^{-1}$ at 22 °C), suggesting that this step is not solvent dependent. By spiking MeCN solutions of **2a** with water, so that the concentration of water in MeCN was ~10 or 100 times the concentration of the Mo complex, the rate of the process remained unaffected. This observation suggests that within the concentration limit, any water present in the solvent does not affect the rate of the reaction.

Interestingly, if **2a** was dissolved in pyridine a red solution was instantly produced, indicating the formation of a pyridine adduct. Complexes of this type have been structurally characterized for the hydrotris(3,5-dimethylpyrazol-1-yl)borate (L) system.[25a] In agreement with this observation, the red compound could also be generated by adding pyridine to the blue MeCN solution, which suggests a higher thermodynamic stability of the pyridine-coordinated complex, as expected from the high donor ability of pyridine. More importantly, this experiment demonstrates that the coordinated MeCN is labile towards substitution, consistent with the exchange of coordinated MeCN with the bulk solvent. The mechanism of pyridine coordination may also be different from the mechanism of acetonitrile coordination, but this was not explored in this investigation.

**Calculated structures**: Calculations were performed on stable species and transition states that are involved in the OAT reaction and in the replacement of the phosphine oxide by the MeCN solvent. The optimized geometries of the species in this reaction are shown in Figure 3.

The comparison of the geometrical data of the calculated **1** reactant (REAC-C, Figure 3) with crystallographic data for $[LMoO_2(SPh)]$[28] and $[L^{iPr}MoO_2(OAr)]$ (OAr = phenolate, naphthalote)[22] shows good agreement. Both the optimized Mo=O bond lengths (1.75 Å) and the optimized Mo–N bond lengths (2.34, 2.21 Å) are slightly longer than the experimental values 1.70 Å and 2.32 and 2.19 Å, respectively, whereas the optimized O-Mo-O angle (103.7°) is similar to the experimental angle (103.4°). In agreement with the experimental results, the Mo–N bonds *trans* to the oxo groups are longer, by 0.13 Å, than the Mo–N bond *trans* to the SPh and OAr groups.

The optimized geometry of the transition state (TS-IC, Figure 3) for the attack of $PMe_3$ on $[L^{iPr}MoO_2(OPh)]$ shows bond lengths that are intermediate between those of the reactant (REAC-C) and $[L^{iPr}MoO(OPh)(OPMe_3)]$ (INT-IC, Figure 3). The Mo–O bond under attack (1.83 Å) is slightly longer than that in the reactant (1.75 Å), but shorter than that in the intermediate (2.21 Å). The O–P bond is beginning to form in the transition state, but is significantly longer in the transition state (2.15 Å) than it is in the intermediate (1.58 Å). In terms of these distances, TS-IC would be an early transition state. In our optimized structure for TS-IC, the torsion angle O-Mo-O-P is −79.6°. This value is in good agreement with previous theoretical work[18] that suggested an angle close to ±90° was necessary to occupy the correct Mo d orbital in the $2e^-$ reduction from $Mo^{VI}$ to $Mo^{IV}$ during OAT. The occupation of this particular metal orbital is associated with the spectator oxygen effect. TS-IC has a large O-P-$C_{Me}$ angle (153.0°), the implications of which will be discussed later. The calculated vibrational frequencies of the completely optimized transition-state geometry show one imaginary frequency ($194i\ cm^{-1}$) with a motion appropriate for this transition state.

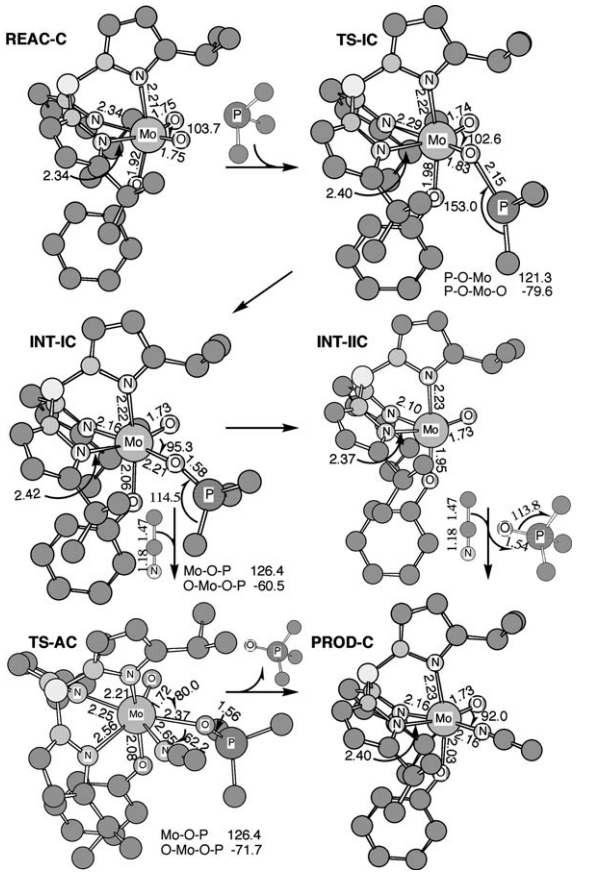


Figure 3. Calculated geometries and metric parameters for the reactants, transition states, intermediates, and product for the OAT reaction of **1** (REAC-C) with $PMe_3$.

Our calculated $[L^{iPr}MoO(OPh)(OPMe_3)]$ intermediate structure (INT-IC, Figure 3), has a well-formed O–P bond and a weaker Mo–$OPMe_3$ dative bond (2.21 Å). The O–P bond in this intermediate is 0.04 Å longer than the corresponding bond in the free ligand, a difference that parallels the formation of a strong Mo–$OPMe_3$ dative bond (see below). In this structure, the difference in the strengths of the three Mo–O bonds can be seen in the *trans* influence on the Mo–N bonds. The calculated bond lengths are in good agreement with the experimental values[20] for **2a**, the "spectator" Mo–O bond has the largest error, but its shortening with respect to REAC is correctly predicted. The O-P-$C_{Me}$ angles (109–115°) are now close to that expected for a phosphine oxide (~115°). The Mo-O-P angle (126.4°) is similar to the experimental value of 132.4°. The calculated O-Mo-O-P torsion angle is −60.5°, also in good agreement with the observed values of −57.5°.

  

The next step in the oxo-transfer reaction, after the formation of the intermediate (INT-IC), is the substitution of phosphine oxide with a molecule of solvent (MeCN in this case) to produce the product (PROD-C). There are two possible "ideal" mechanisms: a two-step dissociative mechanism whereby $OPMe_3$ leaves before MeCN enters; and an associative mechanism whereby MeCN binds to the intermediate (INT-IC) before $OPMe_3$ leaves. For the dissociative mechanism, one expects a five-coordinate intermediate, whereas for a truly associative mechanism, one expects a seven-coordinate intermediate. Of course, exchange pathways that are intermediate between these "ideal" situations are common. In an exchange pathway, the seven-coordinate species would be expected to be a transition state, with the degree of attachment of the exchanging ligands being a measure of the associative or dissociative character. To examine both possible pathways, we calculated the five-coordinate [$L^{iPr}$MoO(OPh)] intermediate (INT-IIC) that one expects in the dissociative mechanism, and a seven-coordinate species (TS-AC) corresponding to an associative exchange mechanism. The square pyramidal, five-coordinated [$L^{iPr}$MoO(OPh)] intermediate (INT-IIC) has a vacant coordination site *trans* to one of the pyrazole nitrogen donors, and this Mo–N bond is now even shorter (2.10 Å) than it was in the intermediate (INT-IC).

In the pathway for the associative mechanism, no seven-coordinate intermediate was found, however, a seven-coordinate transition state (TS-AC) for exchange of $OPMe_3$ with MeCN could be located. In the optimized geometry of TS-AC, there is one imaginary frequency ($64i\ cm^{-1}$) corresponding to the vibration that breaks (makes) the Mo–OP bond and makes (breaks) the Mo–NC bond. The low imaginary frequency is indicative of a very "loose" transition state, in which both $OPMe_3$ and NCMe are nearly dissociated. The Mo–OP bond is longer (2.37 Å) and the O–P bond is shorter (1.56 Å) than those in the intermediate (INT-IC). The Mo–NC bond is longer (2.65 Å) than that of the product (PROD-C), in which MeCN is fully coordinated. In this seven-coordinate TS-AC, the weakest Mo–N (pyrazole) bond, *trans* to the oxo ligand becomes even longer (2.56 Å). A second TS of nearly equal energy exists, in which the entering (MeCN) and leaving ($OPMe_3$) ligands have switched positions.

In the structure of the MeCN-substituted product (PROD-C, Figure 3), the Mo–NC bond is completely formed, with a Mo–NC bond length of 2.16 Å. The Mo–N bond length *trans* to MeCN is similar to that in the intermediate. This similarity in *trans* influence of $OPMe_3$ and MeCN suggests similarities in their Mo–ligand bond strength.

**Calculated energies**: The reaction energies in Table 2 and Figure 4 are all relative to the energy of the reactant (REAC-C) plus the energy of both $PMe_3$ and MeCN. Gas-phase enthalpies and free energies, and solvation-corrected free-energies for MeCN at standard conditions, are given in Table 2. Figure 4 shows the free-energy profile for the predictions in MeCN, which will be described in detail below. The $PMe_3$ substrate reacts by crossing the transition state, TS-IC, to form the intermediate, INT-IC. For TS-IC, the B3LYP gas-phase enthalpic barrier ($\Delta H^{\neq}$) is 37.6 kJ mol$^{-1}$.

Table 2. Calculated energies in kJ mol$^{-1}$. Values in parenthesis are estimated, as discussed in the text.

| | $\Delta H^{o}$ (gas phase) | $\Delta G^{o}$ (gas phase) | $\Delta G^{o}_{solv}$(MeCN) |
|---|---|---|---|
| REAC-C | 0.00 | 0.00 | 0.00 |
| TS-IC | 37.59 | 85.49 | 95.00 |
| INT-IC | −90.25 | −37.98 | −41.02 |
| TS-AC | −12.86 | 84.74 | 101.49 |
| (TS-IIC) | | (71.95) | (68.91) |
| INT-IIC | 19.68 | 13.42 | −11.42 |
| (TS-IIC′) | | (61.54) | (35.14) |
| PROD-C | −56.84 | −14.99 | −41.39 |

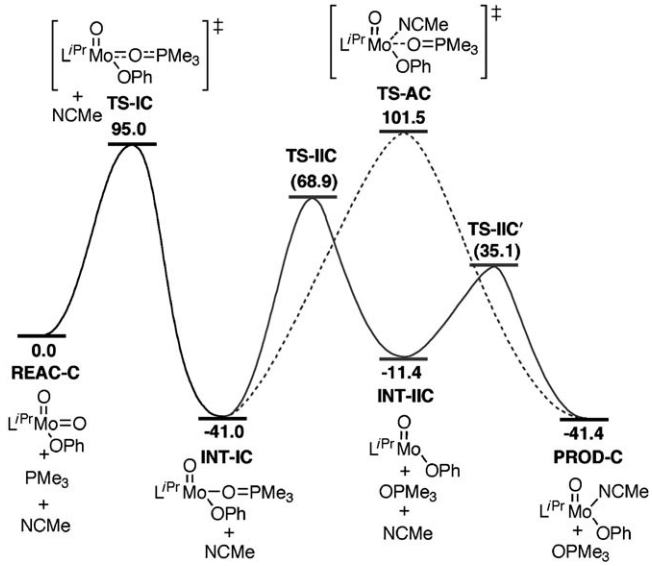


Figure 4. Reaction path for REAC-C+$PMe_3$+MeCN→PROD-C+$OPMe_3$. Solid and dashed lines represent the dissociative and associative paths, respectively, for the solvation of INT-IC. All energies are solvent-corrected (MeCN) free energies, given in kJ mol$^{-1}$. Values in parenthesis are estimated, as discussed in the text.

Gas-phase corrections for the loss in entropy on forming this transition state produce a free-energy barrier ($\Delta G^{\neq}$) of 85.5 kJ mol$^{-1}$. Solvation corrections increase the free-energy barrier ($\Delta G^{\neq}_{solv}$(MeCN)) to 95.0 kJ mol$^{-1}$. Additional corrections for the reduction in entropy due to restricted motion of the separated species in solution[29] were not made. The enthalpy of formation ($\Delta H^{o}$) of INT-IC is −90.3 kJ mol$^{-1}$ and the free energy, $\Delta G^{\neq}_{solv}$(MeCN), of −41.0 kJ mol$^{-1}$ favors its formation, however, the entropy does not. Although the entropy contribution is unfavorable, overall, the intermediate (INT-IC) is found to be quite stable.

Energies for the replacement of the $OPMe_3$ ligand in INT-IC by MeCN were determined for both a dissociative and an associative path. The free-energy barrier for the dissociative path was taken as the dissociation energy of the

  

$OPMe_3$ ligand. The enthalpic differences correspond to an Mo–$OPMe_3$ bond energy of 109.9 kJ mol$^{-1}$. In this dissociative reaction, the entropy is higher because two species are produced. However, this increase in entropy occurs only after most of the enthalpic barrier is achieved. In summary, in determining the free-energy barriers for the dissociative mechanism, the free energy of the dissociative intermediate species (INT-IIC) cannot be used as the barrier. Thus, the maximum free-energy barrier for the dissociative route corresponds to the enthalpic barrier of 109.9 kJ mol$^{-1}$. After formation of INT-IIC, MeCN must overcome an entropic barrier to coordinate to INT-IIC and form the product (PROD). In this "forward" reaction, we assume that the full entropic barrier is encountered before the enthalpic stabilization from the formation of the new Mo–NCMe bond reduces the energy to that of the product. For both of these estimated dissociative transition states, the solvation corrections, like the entropic corrections, correspond to the associative precursor, INT-IC and PROD-C, respectively.

On the associative path, TS-AC has an enthalpic barrier (from the intermediate, INT-IC) of 77.4 kJ mol$^{-1}$. Gas-phase entropic corrections and solvent corrections produce a free-energy barrier ($\Delta G^{\ddagger}_{solv}$(MeCN)) of 142.5 kJ mol$^{-1}$, a barrier that is ~33 kJ mol$^{-1}$ higher than the highest barrier on the dissociative path. The enthalpic data (uncorrected for solvent) suggest that the Mo–$OPMe_3$ bond is ~43 kJ mol$^{-1}$ stronger than the Mo–NCMe bond. However, the large dipole moment of $OPMe_3$ leads to a large solvation correction favoring the replacement of the phosphine oxide by MeCN, an overall reaction that is now favored by 0.4 kJ mol$^{-1}$. The high concentration of MeCN further favors formation of this substituted product (PROD-C).

## Discussion

The results presented demonstrate that the reactions of tertiary phosphines with **1** proceed through multiple transition states; in this case, two transition states were experimentally defined. The first involves the formation of a phosphine oxide-coordinated intermediate, the second one involves the formation of a solvent-coordinated complex. In the context of biological OAT reactions, the formation of a dinuclear species is not pertinent and will not be discussed further, but the other two transition states are relevant.

**Mechanism of formation of 2**: The reaction of **1** with $PEt_3$ or $PPh_2Me$ follows a second-order process. This reaction proceeds as the tertiary phosphine approaches the Mo center, followed by the nucleophilic attack by the tertiary phosphine and the transfer of two electrons to the Mo center. The reaction is dependent on the nature of the phosphine, as evidenced from rates of the reaction: $PPh_2Me$ reacts 3.6 times slower than $PEt_3$ with **1** in MeCN at approximately 12 °C. This slower reaction is consistent with the lower p$K_a$ of $PPh_2Me$ (6.5), relative to that of $PEt_3$ (8.69). Thus, the rate of the reaction leading to the intermediate is strongly influenced by the relative basicity of the attacking phosphine, suggesting that the oxygen has sufficient acidity to react faster with stronger bases. Accordingly, the difference between the enthalpic barriers is large, $(\Delta H^{\ddagger})_{PEt_3}$ = 48.4 kJ mol$^{-1}$ verses $(\Delta H^{\ddagger})_{PPh_2Me}$ = 73.4 kJ mol$^{-1}$.

For both phosphines, the first step in the formation of **2** proceeds by an associative mechanism, as evidenced by the large negative entropies of activation. Furthermore, the enthalpy of activation suggests that there is a significant degree of bond breaking/making in the transition state. Moreover, the relatively low enthalpy of activation, $\Delta H^{\ddagger}$ = 48.4 kJ mol$^{-1}$ for $PEt_3$, is suggestive of the formation of a strong P=O bond at the expense of an Mo=O bond. On the other hand, the $PPh_2Me$ reaction has a significantly larger enthalpy of activation, $\Delta H^{\ddagger}$ = 73.4 kJ mol$^{-1}$, suggesting that the P=O double bond formation is energetically more difficult. Considering that the Mo=O bond in the starting material is the same, this enthalpic difference is likely to reflect a difference in basicity of the phosphines coupled with differences in steric interactions in the transition state.

The calculations predict an associative transition state with a solvent-corrected free-energy barrier of 95.0 kJ mol$^{-1}$ for the reaction of the simpler substrate, $PMe_3$, in reasonable agreement with the experimental results ($\Delta G^{\ddagger}$ = 92.9–94.8 kJ mol$^{-1}$). The calculated structure for this first transition state, TS-IC, suggests that there are two components to its electronic structure. Usually, the attack on the M=O bond by a substrate is thought of as the attack of a nucleophile (the substrate) on the $\pi^*$ M=O orbital, forcing a $2e^-$ reduction of the metal center. Ultimately, of course, this is the final outcome. However, the metal-based oxygen may also act as a nucleophile and attack an empty orbital on the substrate. The surprisingly large O-P-$C_{Me}$ angle[30] (153.0°) suggests that some of this "role reversal" is taking place in TS-IC. If the attack of $PMe_3$ on the Mo=O bond involved only the P lone pair attacking the Mo=O $\pi^*$, one would expect the three-fold axis of $PMe_3$ to be aligned with the axis of attack, P→O. This alignment would produce an idealized O-P-$C_{Me}$ angle of ~115°. On the other hand, if the oxo ligand were the nucleophile and it attacked the phosphine through the P–$C_{Me}$ $\sigma^*$ orbital, phosphorus would become hypervalent (trigonal bipyramid with five valence-electron pairs). The lone pair on phosphorus would occupy an equatorial site in the TBP description. In this alternative case, the idealized O-P-$C_{Me}$ angle would be 180°. Thus, the calculated angle of 153.0°, which is nearly halfway between the two extremes, suggests an intermediate situation with nearly equal mixtures of the two types of nucleophilic attack. As the system proceeds to the intermediate, the O-P-$C_{Me}$ angle decreases to that expected for $OPMe_3$. The changes in the C-P-C angles can also give an indication of the hypervalent character of P in TS-IC. If P has taken on hypervalent character, one would expect the C-P-C angle in the equatorial plane to be larger than the other C-P-C angles. The calculated C-P-C angles for INT-IC are almost equivalent, 106.3, 107.0, and 107.4°, whereas in TS-IC they are 101.0, 101.6, and 103.2°. The difference in these angles is

  

smaller than one would expect for a true five-coordinate hypervalent P, which suggests somewhat less hypervalent character of the P than the O-P-C angle alone.

**Mechanism of loss of $OPR_3$ from 2**: At 5 °C in MeCN, the rate of solvation of **2a** is approximately five times slower than that of **2b**, which underscores the importance of the leaving groups in the rate of the reaction. The free energy of activation is consistent with the rate data, with higher free energy of activation for **2a**. Because the enthalpies of activation are within the error, entropy is the primary contributing factor in the difference in free energy. Very importantly, the entropy of activation for both leaving groups is positive and indicates an overall dissociative mechanism. Of the two leaving groups, $OPPh_2Me$ has a larger gain in conformational flexibility during dissociation than $OPEt_3$, ($\Delta S^{\neq} = 47.3$ and $18.2\ J\,mol^{-1}K^{-1}$, respectively). The larger entropy lowers the free energy of activation for the dissociation of $OPPh_2Me$ by more than that for $OPEt_3$.

The DFT calculations predict that the dissociative route through the five-coordinate intermediate (INT-IIC) is favored over the associative route by $\sim 33\ kJ\,mol^{-1}$. We also calculated a triplet state for the five-coordinated intermediate on the dissociative path. The geometry of this state is trigonal bipyramidal at the molybdenum center. The calculations predict this structure to be several $kJ\,mol^{-1}$ more stable than the singlet. However, it is known that the B3LYP method overestimates the stability of triplet states.[31] Furthermore, no indication of any contribution by a triplet state was observed in the experiments. Thus, we believe that the triplet is less stable than the singlet and, hence, it is not important in this reaction.

Although it is clear that the solvation of the intermediate (i.e., step 2 in Figure 1) follows a dissociative mechanism, the activation parameters alone cannot distinguish between a dissociative interchange or a purely dissociative mechanism. For a purely dissociative mechanism to be operative, the Mo center would need to pass through a pentacoordinate (INT-IIC, Figure 3) species prior to solvent coordination. For a dissociative interchange ($I_d$) mechanism to be operative, the formation of a Mo–solvent bond has to begin before the Mo–OP bond is completely broken, thereby stabilizing the transition state by never allowing the metal center to become truly pentacoordinated. The positive entropy of activation suggests that, in the transition state, bond breaking is more important than bond making. From the predicted high stability of the five-coordinate intermediate and the calculated higher-energy associative reaction path, the calculations support a dissociative mechanism. However, as with the experimental results, the calculations cannot really distinguish between a true dissociative mechanism and a dissociative interchange one, as this choice will be very solvent and substrate dependent. The calculations find a purely dissociative free-energy barrier of $109.9\ kJ\,mol^{-1}$, which is $21.8\ kJ\,mol^{-1}$ higher in energy than the experimental value ($88.1\ kJ\,mol^{-1}$). The larger calculated free-energy barrier is an indication that the loss of phosphine oxide in a solution of MeCN may be better described by a dissociative interchange mechanism.

**The overall reaction profile**: Transformation of **1** to **2** to **3** has two important features associated with the reaction. The first feature pertains to the effect of the substrate upon the rate-limiting step of the reaction. Although the two substrates ($PEt_3$ and $PPh_2Me$) are similar in their geometry about the central phosphorus atom, $PEt_3$ is expected to have a higher conformational flexibility and, as such, leads to a greater entropic penalty (Table 1). On the other hand, $PPh_2Me$ has a lower basicity due to the electron-withdrawing nature of the phenyl rings and is more sterically encumbered, which results in a higher enthalpic contribution and retardation of the reaction. The second feature pertains to the replacement of phosphine oxide by acetonitrile, which is mainly dissociative in nature for both substrates. The rate of loss for the larger phosphine oxide ($PPh_2Me$) is greater, consistent with a steric driving force and a looser transition state, as indicated by the greater entropy of activation (Table 1). The calculations support the identification of this rate-limiting step, however, the calculations also show that the free-energy difference between the barrier to the formation of the phosphine oxide-coordinated intermediate and the barrier of its dissociation is small. Thus, for other substrates and complexes, the rate-limiting step could be different and the nature of the loss of phosphine oxide could change.

Kinetic investigation by Bray and co-workers demonstrated that the formation of the enzyme–substrate complex for DMSO reductase is found to be rate-limiting at pH 5.5, whereas at pH 8.0, the oxo-transfer step has been proposed to be rate limiting.[32] Similarly, in the OAT reactions of W-substituted DMSO, the first electron-transfer step, that is, the formation of the intermediate, is proposed to be the rate-limiting step.[33] Brody and Hille have investigated the atom-transfer chemistry of sulfite oxidase (SO), with sulfite and dimethyl sulfite as substrates.[34] Their interpretation was that the nucleophilic attack, and not product dissociation, was the rate-limiting step. In general, the kinetic studies on the enzymes were focused on the catalytic cycle and, thus, information on the kinetics of the individual steps of the cycle is not available. However, the rate-limiting step can be modulated by the nature of the substrate and the catalytic site, underscoring the importance of subtle perturbations to the reaction mechanism. Although the parallel is compelling, it is not comprehensive, as enzymatic systems are investigated under catalytic conditions and the current work did not focus on establishing a saturation behavior.

## Conclusions

The mechanistic details of the oxygen-atom-transfer reactivity from a dioxo-$Mo^{VI}$ center were investigated, and the overall reaction was described in terms of elementary steps that were experimentally and theoretically defined. The

  

mechanism of the first step involves the combination of a conventional nucleophilic attack by the phosphine on the Mo=O $\pi^*$ orbital and nucleophilic attack by the terminal oxo group on the P–C $\sigma^*$ orbital (evident from the large O-P-$C_{Me}$ angle in TS-IC). The associative transition state of the reaction leads to an intermediate in which the phosphine oxide remains coordinated to the metal center. Next, a solvent molecule replaces the phosphine oxide, leading to the formation of a solvent-coordinated complex. Kinetically, this replacement proceeds through a dissociative transition state (positive entropy of activation) following a dissociative or dissociative interchange pathway. The Mo–$OPMe_3$ bond is enthalpically more stable than the Mo–NCMe bond, however, the high solvent (MeCN) concentration and the large stabilization of the polar product, $OPMe_3$, drives the reaction.

The rate-limiting step was found to be the initial nucleophilic-attack step, in agreement with the DFT calculations. At 298 K, the experimental free-energy difference ($\Delta\Delta G^{\neq}_{298}$) between the two substrates is very small (1.9 kJ mol$^{-1}$) for the nucleophilic-attack step, and it is marginally higher (4.3 kJ mol$^{-1}$) for the following step. The unequal difference in the two steps suggests it may be possible to alter the rate-limiting step by suitable choice of substrate. In light of the kinetic investigation on DMSO reductase, for which rate-limiting steps were noted to be different at different pH, the present work provides a parallel in discrete oxomolybdenum complexes.

## Experimental Section

**Materials and methods**: All compounds were prepared as reported.[20,21] All kinetic investigations were conducted by using a temperature-controlled Cary-14 spectrophotometer operating under an OLIS operating system, or by using a Bruker 300 MHz NMR spectrometer. All mass spectra were collected by using a Micromass ZMD quadrupole spectrometer with MeCN as the mobile phase. All solutions with distilled solvents were prepared under an argon atmosphere by using standard Schlenk techniques and gas-tight syringes.

**Kinetics of the [L$^{i\mathrm{Pr}}$MoO$_2$(OPh)]/PR$_3$ reaction**: The reactions of [L$^{i\mathrm{Pr}}$MoO$_2$(OPh)] (**1**) with $PEt_3$ or $PPh_2Me$ in MeCN or benzene were monitored by performing single-wavelength assays at 910 nm. Fresh stock solutions of **1** were prepared at a concentration of ~2.5 mg mL$^{-1}$ (4.5 mM) and stock $PR_3$ solutions were prepared at a concentration of ~1–2 M. In a typical assay, 750 μL of the **1** stock solution was added to an anaerobic cuvette containing the required amount of solvent so that, after the desired volume of phosphine was added, the final volume would be 1 mL (~3.4 mM of **1**). The ratios of concentrations of $PEt_3$ to **1** were 7.8, 15, 29.8, and 59.7 to maintain pseudo-first-order conditions, whereas those of $PPh_2Me$ to **1** were: 10, 20, 40, and 90. The cuvette was equilibrated to the desired temperature in the sample chamber of the spectrophotometer, whereas the stock $PR_3$ solution was equilibrated separately. Once equilibrated, the desired volume of $PR_3$ solution was added by using a gas-tight syringe, then shaken for 5–10 s and assayed. Each assay was monitored for a time equivalent to 5–8 times the predicted half-life ($t_{1/2}$) of formation, with a typical resolution of one data point per 10 s, and a total of 1024 data points were collected. All single-wavelength assays were fitted to determine the rate constants, and the rate constants were used in calculating the activation parameters from the Eyring and Arrhenius relations, taking account of the concentration of the molybdenum complex.

**Kinetics of [L$^{i\mathrm{Pr}}$MoO(OPh)(OPEt$_3$)] solvation**: The kinetics of solvation of the reaction intermediate **2a** were probed by spectrophotometry. Firstly, time-dependent, multiwavelength scans were collected in two major regions: 1200–500 nm, denoted the low-energy region, and 600–230 nm, denoted the high-energy region. In addition, a typical high-energy experiment was conducted similarly, but to a final concentration of ~375 μM and with scanning from 600–230 nm. Each data set was deconvoluted into three component species by using the singular value decomposition (SVD) technique[35] using Matlab 6.0 and Mathcad 2000I. The first process involves the solvation reaction and a second slower process involves the formation of a dinuclear species; the different time constants offer a reasonable kinetic resolution.

Single-wavelength assays were conducted at 301, 680, and 910 nm. A typical single-wavelength experiment involved the equilibration of solvent, cuvette, and sample cell, the choice of an appropriate number of data points (~400 and 1000), and total assay time (~5.5–6 times the predicted $t_{1/2}$ of the exponential decay). The rate constants were determined by fitting the data as either a single (910 and 301 nm, for which there was no difference in the absorption spectra of the solvated and dinuclear species) or double exponential (680 nm, for which the dinuclear species exhibit a different absorption profile). Single-wavelength spectrophotometric measurements at 680 nm were conducted in MeCN, benzene, THF, and deoxygenated MeCN/water mixtures (10 and 100 fold excess with respect to the molybdenum complex). The activation parameters for the conversion of **2a** to **3** were determined from the Eyring and Arrhenius relations.

The dissociation in [$D_6$]benzene and [$D_3$]MeCN of the phosphine oxide was also probed by $^1$H and $^{31}$P NMR spectroscopy. A typical sample was prepared by dissolving 10 mg ($1.6\times10^{-5}$ mol) of **2a** in 700 μL of the dry solvent (cold and dry in the case of MeCN) in the dry-box followed by analysis within 2 min. Once the initial spectrum was recorded, the sample was immediately incubated at 11 °C for 5 min before returning to record the subsequent spectrum. The terminal time point was collected after 24 h. The integrated areas of $^{31}$P resonances were used for single exponential fits to determine the rate of phosphine oxide release.

**Kinetics of [L$^{i\mathrm{Pr}}$MoO(OPh)(OPPh$_2$Me)] solvation**: The kinetics studies of solvation of **2b** were carried out as described for **2a**; the only change observed was the shift of the 910 nm band to ~900 nm; in this case, two exponents were used to obtain kinetic parameters.

**Theoretical details**: The theoretical model system used in this work consisted of the full **1** reactant and $PMe_3$ as a model substrate, rather than $PEt_3$ or $PPh_2Me$, as used in the experiments. The geometries of all structures for the theoretical model system were fully optimized by the B3LYP[36] DFT[37] method, as implemented in Gaussian 98 or Gaussian 03.[38] Analytical harmonic frequencies were calculated for all stationary points to confirm the nature of these points, for the zero-point energies, and for the thermodynamic properties. Solvation corrections in MeCN were performed by using the polarizable continuum model (PCM) method,[39] as implemented in Gaussian 03. The results reported in this work were obtained with a standard valence double-$\zeta$ quality basis set (D95 V)[40] for B, C, N, O, and H. A small effective core potential (ECP)[41] was used for Mo (1s2s2p3s3d) with a double-$\zeta$ quality basis set that includes the outer 5p function developed by Couty and Hall.[42] An ECP (1s2s2p) with a double-$\zeta$ quality basis set (LANL2DZ)[43] was used for P, and to properly describe the hypervalent character of P, a polarization function with an exponent of 0.340 was added.[44]

## Acknowledgements

We thank Mr. S. Davie and Drs. P.D. Smith, C.J. Doonan, and V. Nemykin for experimental assistance, and Prof. J.H. Espenson for discussions. We would also like to thank the Laboratory for Molecular Simulation and the Supercomputing Facility at Texas A&M University for providing software and computer time for the theoretical calculations. Financial support of this research from the National Institutes of Health GM 061555-02 (P.B.), the Australian Research Council (C.G.Y.), Foundation of the Serbian Ministry of Science, 1795 and 142037 (S.D.Z.), Welch Foundation A 648 (M.B.H.), National Science Foundation CHE 9800184

  

and 0518074 (M.B.H.), and National Science Foundation DMS 0216275 (M.B.H.) is gratefully acknowledged.

[1] H. Taube, *ACS Symp. Ser.* **1982**, *198*, 151–179.
[2] K. B. Sharpless, *Tetrahedron* **1994**, *50*, 4235–4258.
[3] R. H. Holm, *Chem. Rev.* **1987**, *87*, 1401–1449.
[4] L. K. Woo, *Chem. Rev.* **1993**, *93*, 1125–1136.
[5] J. H. Espenson, *Adv. Inorg. Chem.* **2003**, *54*, 157–202.
[6] B. S. Lane, K. Burgess, *Chem. Rev.* **2003**, *103*, 2457–2473.
[7] W. A. Nugent, T. V. RajanBabu, M. J. Burk, *Science* **1993**, *259*, 479–483.
[8] R. H. Holm, *Coord. Chem. Rev.* **1990**, *100*, 183–221.
[9] J. H. Enemark, C. G. Young, *Adv. Inorg. Chem.* **1993**, *40*, 1–88.
[10] J. H. Enemark, J. J. A. Cooney, J.-J. Wang, R. H. Holm, *Chem. Rev.* **2004**, *104*, 1175–1200.
[11] C. G. Young in *Biomimetic Oxid. Catal. Transition Met. Complexes* (Ed.: B. Meunier), Imperial College Press, **2000**, Chapter 9, pp. 415–459.
[12] a) R. Barral, C. Bocard, I. Seree de Roch, L. Sajus, *Tetrahedron Lett.* **1972**, 1693–1696; b) M. S. Reynolds, J. M. Berg, R. H. Holm, *Inorg. Chem.* **1984**, *23*, 3057–3062.
[13] a) S. K. Das, P. K. Chaudhury, D. Biswas, S. Sarkar, *J. Am. Chem. Soc.* **1994**, *116*, 9061–9070; b) H. Oku, N. Ueyama, M. Kondo, A. Nakamura, *Inorg. Chem.* **1994**, *33*, 209–216.
[14] a) K.-M. Sung, R. H. Holm, *J. Am. Chem. Soc.* **2002**, *124*, 4312–4320; b) K.-M. Sung, R. H. Holm, *J. Am. Chem. Soc.* **2001**, *123*, 1931–1943; c) J. P. Donahue, C. R. Goldsmith, U. Nadiminti, R. H. Holm, *J. Am. Chem. Soc.* **1998**, *120*, 12869–12881.
[15] B. S. Lim, R. H. Holm, *J. Am. Chem. Soc.* **2001**, *123*, 1920–1930.
[16] a) Z. Xiao, C. G. Young, J. H. Enemark, A. G. Wedd, *J. Am. Chem. Soc.* **1992**, *114*, 9194–9195; b) Z. Xiao, M. A. Bruck, J. H. Enemark, C. G. Young, A. G. Wedd, *Inorg. Chem.* **1996**, *35*, 7508–7515.
[17] V. N. Nemykin, S. R. Davie, S. Mondal, N. Rubie, M. L. Kirk, A. Somogyi, P. Basu, *J. Am. Chem. Soc.* **2002**, *124*, 756–757.
[18] M. A. Pietsch, M. B. Hall, *Inorg. Chem.* **1996**, *35*, 1273–1278.
[19] A. K. Rappé, W. A. Goddard III, *J. Am. Chem. Soc.* **1982**, *104*, 3287–3294.
[20] P. D. Smith, A. J. Millar, C. G. Young, A. Ghosh, P. Basu, *J. Am. Chem. Soc.* **2000**, *122*, 9298–9299.
[21] A. J. Millar, C. J. Doonan, P. D. Smith, V. N. Nemykin, P. Basu, C. G. Young, *Chem. Eur. J.* **2005**, *11*, 3255–3267.
[22] C. J. Doonan, A. J. Millar, D. J. Nielsen, C. G. Young, *Inorg. Chem.* **2005**, *44*, 4506–4514.
[23] V. N. Nemykin, J. Laskin, P. Basu, *J. Am. Chem. Soc.* **2004**, *126*, 8604–8605.
[24] V. N. Nemykin, P. Basu, *Inorg. Chem.* **2005**, *44*, 7494–7502.
[25] a) Z. Xiao, M. A. Bruck, J. H. Enemark, C. G. Young, A. G. Wedd, *Inorg. Chem.* **1996**, *35*, 7508–7515; b) Z. Xiao, C. G. Young, J. H. Enemark, A. G. Wedd, *J. Am. Chem. Soc.* **1992**, *114*, 9194–9195.
[26] C. E. Webster, M. B. Hall, *J. Am. Chem. Soc.* **2001**, *123*, 5820.
[27] A. Thapper, R. J. Deeth, E. Nordlander, *Inorg. Chem.* **2000**, *41*, 6695–6702.
[28] Z. Xiao, M. A. Bruck, C. Doyle, J. H. Enemark, C. Grittini, R. W. Gable, A. G. Wedd, C. G. Young, *Inorg. Chem.* **1995**, *34*, 5950–5962.
[29] Y. B. Yu, *J. Phys. Chem. B* **2003**, *107*, 1721.
[30] In previous theoretical work (ref. [18]), the O-P-C angles were fixed and, therefore, a large O-P-C angle was not observed in the transition state.
[31] Y. Fan, M. B. Hall, *Chem. Eur. J.* **2004**, *10*, 1805–1814.
[32] B. Adams, A. T. Smith, S. Bailey, A. G. McEwan, R. C. Bray, *Biochemistry* **1999**, *38*, 8501–8511.
[33] L. J. Stewart, S. Bailey, D. Collison, G. A. Morris, I. Preece, C. D. Garner, *ChemBioChem* **2001**, *2*, 703–706.
[34] M. S. Brody, R. Hille, *Biochim. Biophys. Acta* **1995**, *1253*, 133–135.
[35] E. R. Henry, J. Hofrichter, *Methods Enzymol.* **1992**, *210*, 129–191.
[36] a) A. D. Becke, *J. Chem. Phys.* **1993**, *98*, 5648–5652; b) C. Lee, W. Yang, R. G. Parr, *Phys. Rev. B* **1988**, *37*, 785–789.
[37] R. G. Parr, W. Yang, *Density-Functional Theory of Atoms and Molecules*, Oxford University Press, Oxford **1989**.
[38] Gaussian 98 (Revision A11), Gaussian 03 (Revision B5), M. J. Frisch, G. W. Trucks, H. B. Schlegel, G. E. Scuseria, M. A. Robb, J. R. Cheeseman, J. A. Montgomery, Jr., T. Vreven, K. N. Kudin, J. C. Burant, J. M. Millam, S. S. Iyengar, J. Tomasi, V. Barone, B. Mennucci, M. Cossi, G. Scalmani, N. Rega, G. A. Petersson, H. Nakatsuji, M. Hada, M. Ehara, K. Toyota, R. Fukuda, J. Hasegawa, M. Ishida, T. Nakajima, Y. Honda, O. Kitao, H. Nakai, M. Klene, X. Li, J. E. Knox, H. P. Hratchian, J. B. Cross, C. Adamo, J. Jaramillo, R. Gomperts, R. E. Stratmann, O. Yazyev, A. J. Austin, R. Cammi, C. Pomelli, J. W. Ochterski, P. Y. Ayala, K. Morokuma, G. A. Voth, P. Salvador, J. J. Dannenberg, V. G. Zakrzewski, S. Dapprich, A. D. Daniels, M. C. Strain, O. Farkas, D. K. Malick, A. D. Rabuck, K. Raghavachari, J. B. Foresman, J. V. Ortiz, Q. Cui, A. G. Baboul, S. Clifford, J. Cioslowski, B. B. Stefanov, G. Liu, A. Liashenko, P. Piskorz, I. Komaromi, R. L. Martin, D. J. Fox, T. Keith, M. A. Al-Laham, C. Y. Peng, A. Nanayakkara, M. Challacombe, P. M. W. Gill, B. Johnson, W. Chen, M. W. Wong, C. Gonzalez, J. A. Pople, Gaussian, Inc., Pittsburgh PA, **2003**.
[39] M. Cossi, N. Rega, G. Scalmani, V. Barone, *J. Chem. Phys.* **2002**, *117*, 43–54.
[40] T. H. Dunning, Jr., P. J. Hay in *Modern Theoretical Chemistry* (Ed.: H. F. Schaefer III), Vol. 3, Plenum, New York, **1976**, pp. 1–28.
[41] P. J. Hay, W. R. Wadt, *J. Chem. Phys.*, **1985**, *82*, 299–310.
[42] M. Couty, M. B. Hall, *J. Comput. Chem.* **1996**, *17*, 1359–1370.
[43] P. J. Hay, W. R. Wadt, *J. Chem. Phys.* **1985**, *82*, 270–283.
[44] S. Huzinaga, *Gaussian Basis Sets for Molecular Calculations*, Elsevier, Amsterdam, **1984**.

Received: February 25, 2006
Published online: July 25, 2006

  